Journal of Applied Polymer Science

Surface Imprinted Core-Shell Nanorod with Ultrathin Water-Compatible Polymer Brushes for Specific Recognition and Adsorption of Sulfamethazine in Water Medium

Jiangdong Dai,[1] Zhiping Zhou,[1] Yongli Zou,[2] Xiao Wei,[1] Xiaohui Dai,[3] Chunxiang Li,[3] Yongsheng Yan[3]

[1]School of Material Science and Engineering, Jiangsu University, Zhenjiang 212013, China
[2]School of the Environment and Safety Engineering, Jiangsu University, Zhenjiang 212013, China
[3]School of Chemistry and Chemical Engineering, Jiangsu University, Zhenjiang 212013, China
Correspondence to: Y. S. Yan (E-mail: ujs2013txh@163.com)

ABSTRACT: A surface imprinted core-shell nanorod with water-compatible property was first prepared, using a two-step "living" polymerization technique, with magnetic attapulgite (MATP) as core, and it was applicable in the enhanced selective removal of sulfamethazine residue from pure water environments. MATP was synthesized by an impregnation and pyrolysis method, and polymerable group was subsequently attached onto the surface. The imprinted polymer nanoshell (13 nm) with the "living" fragments was formed via a reverse atom transfer radical precipitation polymerization, avoiding the tedious graft of initiator and providing the easy-accessible imprinted sites. Ultrathin hydrophilic polymer brushes (2.0 nm) were surface-grafted to improve their water-compatibility. The nanoadsorbent exhibited good thermal stability, magnetism, and hydrophilicity through characterization. The nanoadsorbent showed large adsorption capacity toward sulfamethazine from water, which increased with the increase of contact temperature. Langmuir isotherm fitted the equilibrium data better, and the kinetic data (within 45 min) were well-analyzed by the pseudo-second-order kinetic model. Also, the specific adsorption property of the nanoadsorbent was greatly improved through the surface-grafting, which exhibited excellent selectivity to sulfamethazine compared with other reference antibiotics. Efficient magnetic separation and good reuse of the nanoadsorbent provided the potential possibility for selective recognition and fast removal of antibiotic pollutions from water environments. © 2014 Wiley Periodicals, Inc. J. Appl. Polym. Sci. **2014**, *131*, 40854.

KEYWORDS: adsorption; nanoparticles; nanowires and nanocrystals; radical polymerization; separation techniques; surfaces and interfaces

Received 24 February 2014; accepted 13 April 2014
DOI: 10.1002/app.40854

INTRODUCTION

Sulfonamide antimicrobials (SAs), typically such as sulfadiazine, sulfamerazine, and sulfamethazine (SMZ), have been widely used in human therapy, livestock production, and aquaculture as efficacious medicines for prevention/treatment of diseases or growth promotion.[1] Because SAs are poorly absorbed or metabolized in the intestine as well as domestic and hospital waste, more and more remnants enter into groundwater and soil and are cumulated through the food chain, finally threatening human health. Exposures to residues of sulfonamides and their transformed products might cause allergy, carcinogenesis, or antibiotic resistance.[2] However, due to the extremely low concentration, current treatment technologies hardly remove SAs residue from environment so that more effective methods are importantly needed to be developed. In the recent decade, molecularly imprinted polymers (MIPs) have been commonly applied to remove pollutions including SAs from water environments.[3,4]

Molecularly imprinting technology has been developed into a ripe technology for mimicking natural receptors and obtaining artificial host systems with predetermined binding sites for targeted molecules.[5] The process typically involves the copolymerization of functional and cross-linker monomers in the presence of template molecules in a suitable solvent through noncovalent or covalent interactions. After template removal from the cross-linked polymer matrix, MIPs can be finally obtained with active cavities matched with target molecules in size, structure, and chemical functionality, and show high affinity simulating natural antibody-antigen systems.[6] The characteristics (such as excellent mechanical, stability, ease of preparation, and low cost)

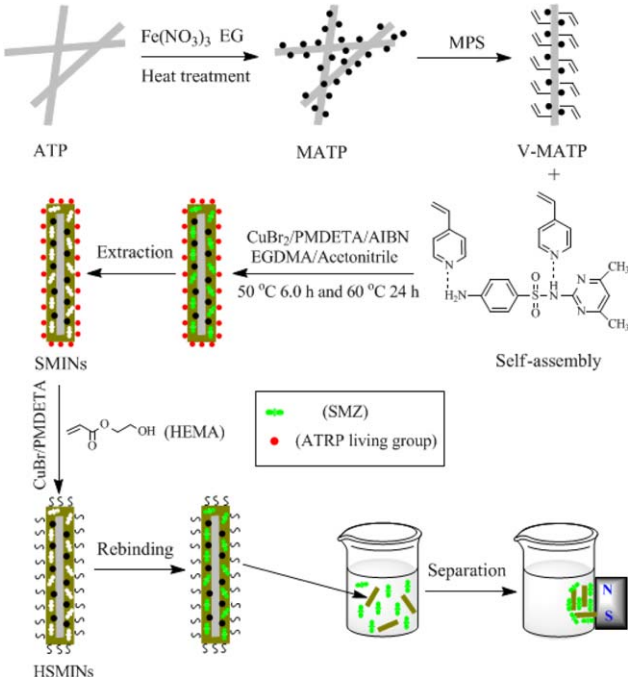

Figure 1. Scheme of synthetic procedure for surface imprinted core-shell nanomaterial with ultrathin hydrophilic polymer brushes. [Color figure can be viewed in the online issue, which is available at wileyonlinelibrary.com.]

make MIPs being widely used in various applications including separation,[7,8] solid phase extraction,[9–11] immunoassay,[12] chemical sensors,[13] drug delivery,[14] and catalysis.[15] Recently, surface imprinting techniques have been progressively explored to address the limitation of bulk MIPs, such as incomplete template removal, low rebinding capacity, poor site accessibility, and irregular materials shape,[16–18] by controlling the template molecules located at the surface or in the proximity of solid materials surface. Popularly, the thin layer of MIPs was grafted at the surface of solid supports to form core-shell structural MIPs, such as monodispersed polystyrene,[19] silica spheres,[20] Fe_3O_4 particles,[21] carbon nanotubes,[22] and natural minerals.[23]

Among attapulgite (ATP) is a natural fibrillar hydrated magnesium silicate mineral with 20–70 nm in diameter and about 0.5–2.0 μm in length.[24] Because of its large specific surface area and abundant reactive-OH groups on the surface as well as its stability, low cost, and ready availability, ATP has been widely used in adsorbents, drilling fluids, paints, adhesives, and supports.[25] An effective approach for enhancing its separability, adsorption capacity and selectivity is the surface functionlization of ATP. To achieve fast separation and recovery, magnetic nanoparticles can be located at the surface to form magnetic attapulgite (MATP), which can be conveniently separated from liquid by an external magnetic field. The surface of MATP is functionalized with thin MIP layers to form magnetic core-shell structures, which possess both magnetism and specific recognition property without any complicated centrifugation or filtration steps. ATP and its functionalized nanocomposites are ideal materials as core matrix.

Up to now, core-shell MIPs have mostly been prepared by seed emulsion polymerization[26] and surface-grafting polymerization.[27,28] Emulsion polymerization is an efficient technique to synthesize core-shell-type particles, but the surfactants can remain on the surface and reduce selectivity toward targets. Generally, the thin imprinted layer could be coated onto the surface of nanoparticles by the grafting approaches, which involve that the polymer layer is built up *in situ* from the pendant polymerable and initiating sites, which are chemically attached onto the surface. The application of the "grafting from" strategy in the field of core-shell MIPs has been greatly promoted benefiting from the progress in the controlled/"living" radical polymerization techniques, such as iniferter-induced "living" radical polymerization (ILRP),[29] reversible addition fragmentation chain transfer (RAFT) polymerization,[30]and atom transfer radical polymerization (ATRP).[31] Among ATRP has widely attracted interest in the preparation of MIPs with improved properties, due to the homogeneous network structure and availably specific post-functionalities as well as its tolerance for a wide range of monomers, templates, and reaction conditions.[32] Many groups have reported the successful molecular imprinting on the surfaces of gold-coated silica wafers,[33] silica gel,[34] magnetic nanoparticles,[35] and anodic alumina oxide membrane[36] using surface-initiated ATRP. However, the modifications of surface-initiated agents commonly require multistep reactions and remain complicated and irreproducible. As an alternative mean, the polymerization

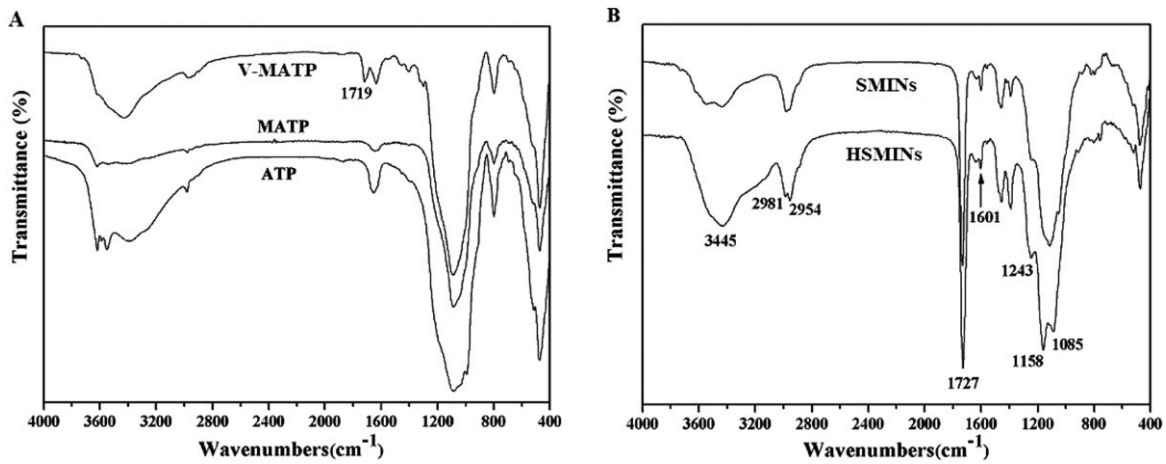

Figure 2. FT-IR spectra of ATP, MATP, and V-MATP (A) and SMINs and HSMINs (B).

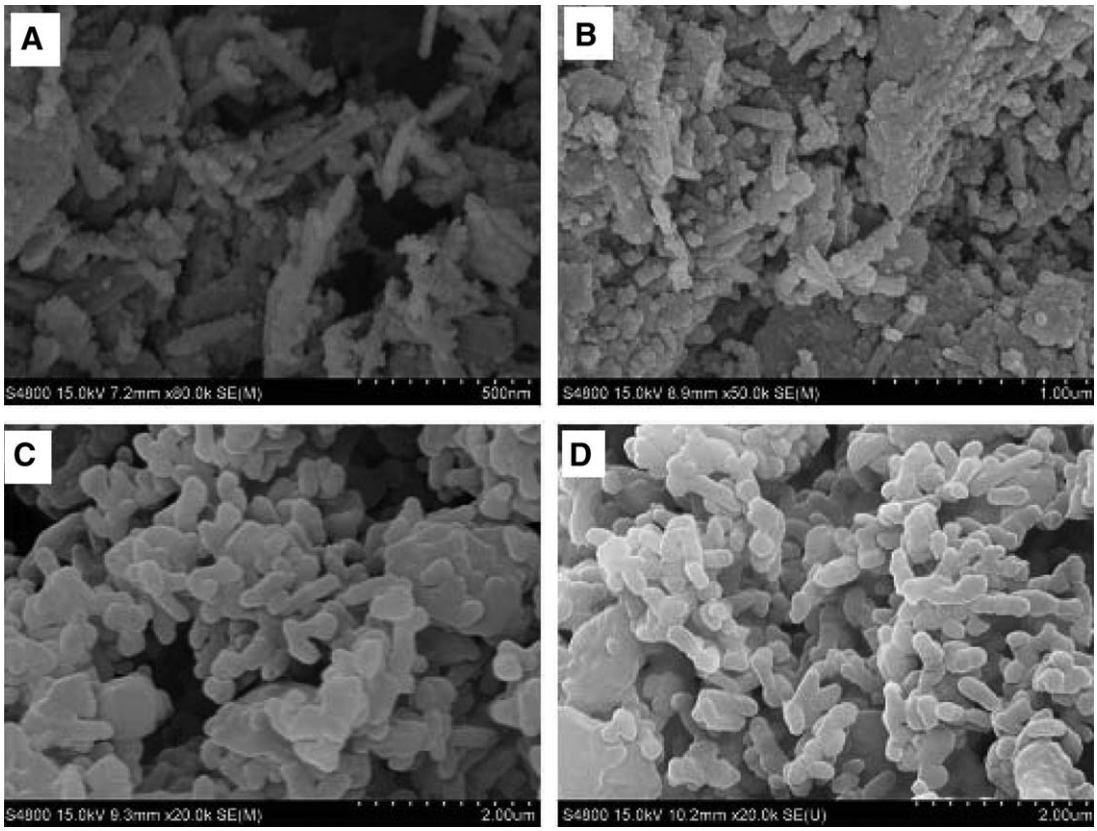

Figure 3. SEM images of ATP (A), MATP (B), SMINs (C) and HSMINs (D).

occurred *in situ* to obtain core-shell MIPs, where polymerable monomers were easily located onto the surface using a one-step reaction. In our previous study, the imprinted polymers were also formed on the surface of vinyl-modified magnetic nanoparticels via atom transfer radical emulsion polymerization.[37] Compared with normal ATRP, reverse atom transfer radical polymerization (RATRP) emerged as a more convenient method, which involves that halogenated Cu (II) is used as a catalyst instead of easily oxidized halogenated Cu (I).[31] Moreover, conventional radical initiators like azobis (isobutyronitrile) can be used, which are cheaper and costless. To our knowledge, there were rare reports on the use of RATRP in the molecular imprinting field, especially for the core-shell MIPs.

The development of molecular imprinting has been greatly made, but many challenges still remain to be dissolved. Particularly, the previously developed MIPs are commonly only organic solvent-compatible and mostly fail to exhibit selective recognition in the pure water, thus remarkably limiting their practical applications, especially in the biotechnology field. There are two strategies to improve surface hydrophilicity, namely involving in the copolymerization of hydrophilic monomers (such as 2-hydroxyethyl methacrylate [HEMA] and acrylamide) in the imprinted polymerization[38] and post-modification of the preformed MIPs.[39] The former strategy is relatively simple, however, requires complicated/time-consuming optimization of formulation parameters influencing MIPs' performance. In contrast, the latter one, mainly by surface-grafting of hydrophilic polymers, has proven high interest because it not only improves surface hydrophilicity but also avoids destroying the efficiency of imprinting sites. Oxelbark et al. reported that surface imprinted core-shell particles with an additional hydrophilic layer were synthesized via surface-initiated ILRP, with molecular recognition ability in organic solvent/buffer mixtures.[40] Pan et al. described the successful preparation of pure-water-compatible imprinted microspheres by the controlled grafting of hydrophilic polymer layers onto the preformed imprinted particles, via surface-initiated RAFT.[41] To our knowledge, however, there were rare reports to date on the preparation of MIPs with pure water-compatible property by the surface-grafting of hydrophilic polymer brushes through ATRP.

The objective of this work is to obtain a novel surface imprinted core-shell nanoadsorbent with hydrophilic polymer brushes (synthesis route in Figure 1), in which MATP was used as core. Magnetic nanoparticles were first attached in the pretreated ATP by the impregnation and pyrolysis method. Then, vinyl groups were introduced onto the surface of MATPs via a silanization reaction. Subsequently, the thin imprinted layer was coated *in situ* on the surface of modified MATPs through reverse atom transfer radical precipitation polymerization (RATRPP) with surface imprinting technique, in which SMZ was used as template molecule, 4-vinylpyridine (4-VP) as functional monomer, ethylene glycol dimethacrylate (EGDMA) as cross-linking agent, copper (II) bromide ($CuBr_2$) as catalysis, and AIBN as initiator. Finally, the hydrophilic polymer brushes

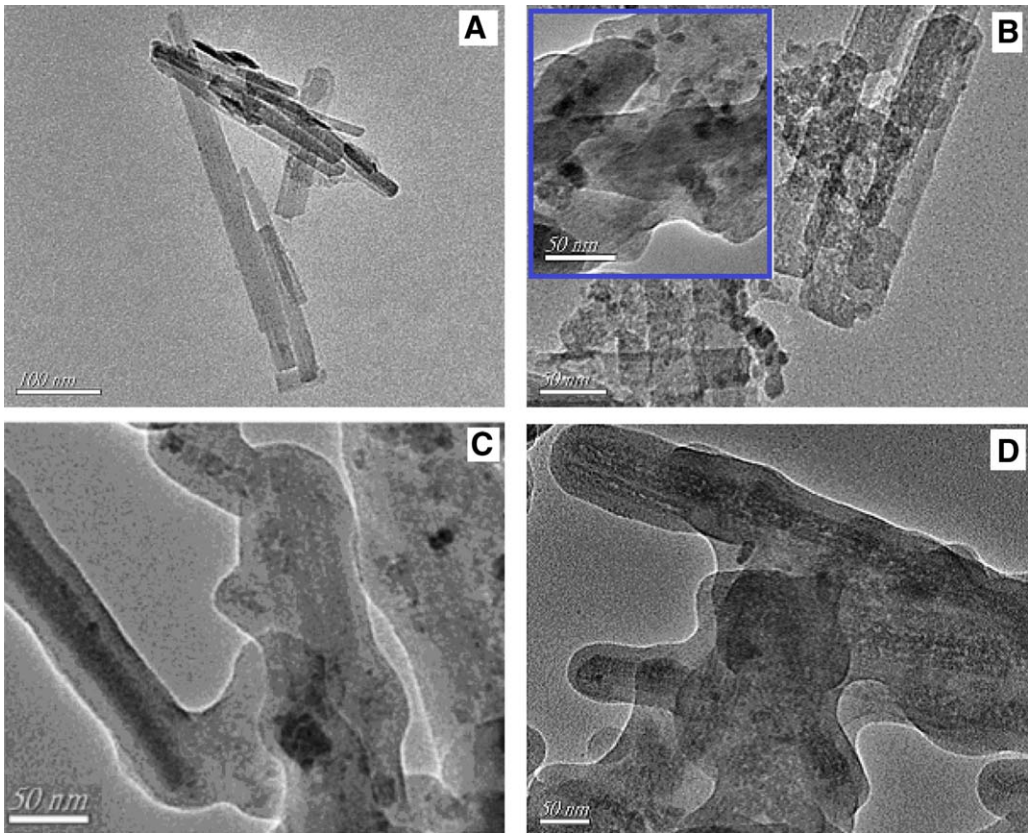

Figure 4. TEM images of natural ATP (A), MATP (B), SMINs (C) and HSMINs (D). [Color figure can be viewed in the online issue, which is available at wileyonlinelibrary.com.]

were grafted from the "living" initiating sites of obtained imprinted nanomaterials to enhance water-compatibility via surface-initiated normal ATRP. The products were characterized by Fourier transform infrared (FT-IR), scanning electron microscope (SEM), transmission electron microscope (TEM), vibrating sample magnetometer (VSM), X-ray Diffractometer (XRD), and Thermogravimetric analysis (TGA). Moreover, their adsorption equilibrium, kinetics, selectivity, and reusability properties in pure water were investigated as well.

EXPERIMENTAL

Materials

Toluene, acetic acid, acetonitrile, methanol, ethanol, ethylene glycol, $CuBr_2$, copper (I) bromide (CuBr), iron (III) nitrate nonahydrate ($Fe(NO_3)_3{\cdot}9H_2O$), and AIBN were purchased from Sinopharm Chemical Reagent Co. (Shanghai, China). EGDMA, 4-VP, HEMA, SMZ, *N*, *N*, *N*′, *N*′, *N*″-pentamethyl diethyenetriamine (PMDETA), 3-(trimethoxysilyl) propylmethacrylate (MPS), tetracycline (TC), ciprofloxacin hydrochloride (CIP), chlortetracycline hydrochloride (CTC), and cefalexin (CFX) were obtained from Aladdin Reagent Co. (Shanghai). ATP was offered by Aotebang International Co. (Huaian, China). Deionized ultrapure water was purified via a Purelab ultra (Organo, Tokyo, Japan).

Characterization and Instruments

FT-IR spectra of prepared samples were measured by a Nicolet NEXUS-470 FTIR apparatus using KBr pellets. A Rigaku D/max-γB XRD was used to identify the crystalline phase via monochromatized with Cu Kα radiation over the 2θ range of 20–80° at a scanning rate of 0.02 deg s^{-1}. The SEM (JEOL, JSM-7001F) and TEM (JEOL, JEM-2100) were used to observe the morphology and size of particles. The saturation magnetization of the magnetic products was determined via a VSM (HH-15, China) under a magnetic field up to 10 kOe. TGA was measured by a DSC/DTA-TG (STA 449C Jupiter, Netzsch, Germany). The water contact angle was determined via a KSV CM200 contact angle instrument (Finland). A UV-2450 UV-vis spectrophotometer (Shimadzu Corporation, Japan) was used to detect the concentration via corresponding absorbance. A reverse-phase HPLC system (Agilent 1200 series) was equipped with a UV-vis detector to achieve the simultaneous detection of several components.

Pretreatment and Purification of ATP

The raw ATP was pretreated and purified via acid treatment to improve surface property. Briefly, 1.0-g attapulgite was treated with 100 mL of 3.0-M HCl solution at 80°C for 2.0 h, and cooled to room temperature. The suspension was filtered using cellulose filter paper under reduced pressure and was thoroughly washed with deionized water to neutral, and was then dried at 60°C for 12 h for further use.

Synthesis of MATP

MATP was synthesized via the impregnation and pyrolysis method.[42] In brief, Fe $(NO_3)_3{\cdot}9H_2O$ (0.6 g) and ATP (1.0 g) were added into 20 mL of ethanol in a flask. The mixture was dispersed

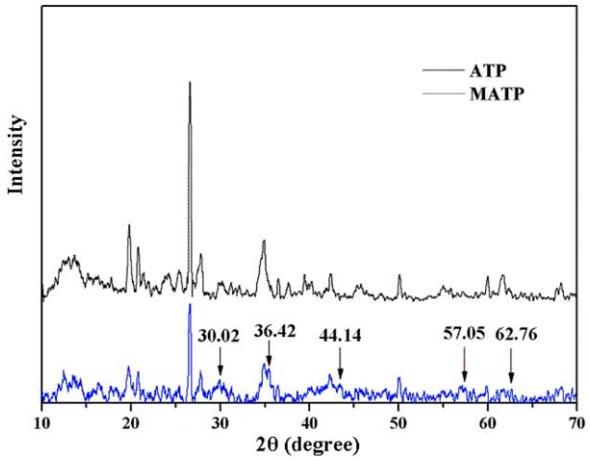

Figure 5. X-ray diffraction patterns of ATP and MATP. [Color figure can be viewed in the online issue, which is available at wileyonlinelibrary.com.]

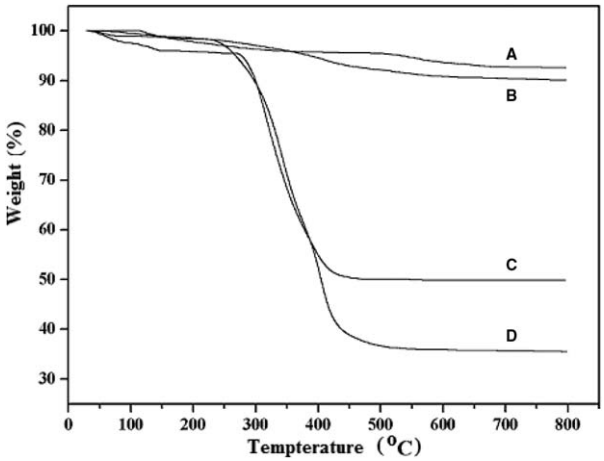

Figure 6. TGA curves of MATP (A), V-MATP (B), SMINs (C) and HSMINs (D). [Color figure can be viewed in the online issue, which is available at wileyonlinelibrary.com.]

under ultrasound for 30 min with the power of 500 W and was stirred vigorously overnight at room temperature, and then was dried at 90°C to remove ethanol for 2.0 h. After that, the powder was dipped with ethylene glycol (2.0 mL), and subsequently was heated at 400°C for 2.0 h in tube furnace with the protection of nitrogen (with heating rate of 5.0°C min^{-1}). Finally, the resulting product was washed with ethanol for three times and was dried at 60°C, and the black powder was obtained.

Preparation of Modified MATP

The surface modification of MATP was carried out via a silanization reaction. MATP (1.0 g) was dispersed into toluene (100 mL) in a round bottom flask (250 mL) by ultrasound for 30 min with the power of 500 W. Then, MPS (3.0 mL) was added into the mixture and the flask was kept at 90°C for 24 h under moderate stirring. After that, the product was collected and washed with ethanol. Then, the vinyl-modified MATP (V-MATP) was obtained after drying at 60°C under vacuum.

Synthesis of Surface Imprinted Core-Shell Nanorod with "Living" Fragments

The thin imprinted polymers were grafted onto the surface of V-MATP via RATRPP as following procedure: 4-VP (34 μL), SMZ (22.6 mg), and EGDMA (0.254 mL) were added into acetonitrile (60 mL) in a one-neck round-bottom flask for self-assembly overnight at room temperature. V-MATP (0.1g) was dispersed into the mixture under ultrasound, and then, $CuBr_2$ (5.6 mg), PMDETA (10.5 μL) and AIBN (12.5 mg) were added into the reaction system, respectively. The system was deoxygenized with nitrogen for 0.5 h and sealed. The flask was placed in water bath oscillator with a rotation rate of 120 rpm at 50°C for 6.0 h, then 60°C for 24 h. The product was collected and thoroughly washed with ethanol, and was then dried at 60°C. Finally, the obtained nanomaterials were purified through Soxhlet extraction with methanol/acetic acid (9/1, v/v) to removal template until no SMZ was determined by UV-vis (at 240 nm). After being dried at 60°C, surface imprinted core-shell nanocomposites with "living" fragments (SMINs) were obtained. The corresponding nonimprinted nanocomposites (SNINs) were prepared by the similar process without the addition of template molecule.

Surface-Grafting of Ultrathin Hydrophilic Polymer Brushes from SMINs

The SMINs with ultrathin hydrophilic polymer brushes were synthesized via surface-initiated normal ATRP according to the following procedure: HEMA (1.5 mL) was added into a 25 mL round-bottom flask with a mixture of methanol (2.0 mL) and water (2.0 mL). CuBr (10.47 mg) and PMDETA (45.8 μL) were placed into the flask in succession under the protection of nitrogen, and subsequently SMINs (100 g) was dispersed into the reaction system. After that, the flask was sealed and heated in a thermostated water bath at 40°C under the stir for 24 h. The SMINs with ultrathin hydrophilic polymer brushes (HSMINs) were collected under a magnet, washed with methanol thoroughly and were then dried at 60°C. The SMINs with ultrathin hydrophilic polymer brushes (HSNINs) was also synthesized via the same method.

Adsorption Experiment

To test the adsorption capability of HSMINs toward SMZ, batch adsorption experiments were performed via the following procedure: 5.0 mg of HSMINs was placed in 10 mL of SMZ aqueous solutions with various concentrations from 5.0 to 150 μmol L^{-1}. After complete reaction at three different temperatures (25–45°C), the supernatant liquids were obtained by magnetic separation, the free concentrations of which were then tested using UV-vis at 239 nm. Also, 5.0 mg of SMINs, SNINs, HSMINs, and HSNINs was added into 10 mL of SMZ solutions (50 μmol L^{-1}) using water and acetonitrile as solvent for 24 h, respectively.

Adsorption kinetics experiments were performed to study the adsorption rate and mechanism of the prepared nanocomposites toward SMZ. HSMINs of 5.0 mg or HSNINs were placed in 10 mL of SMZ solutions with concentrations of 100 μmol L^{-1} at the different interval time, and then, the separated supernatant liquid was determined.

The selectivity experiments were executed via adding 5.0-mg HSMINs/HSNINs into the solutions of single- and double-antibiotics

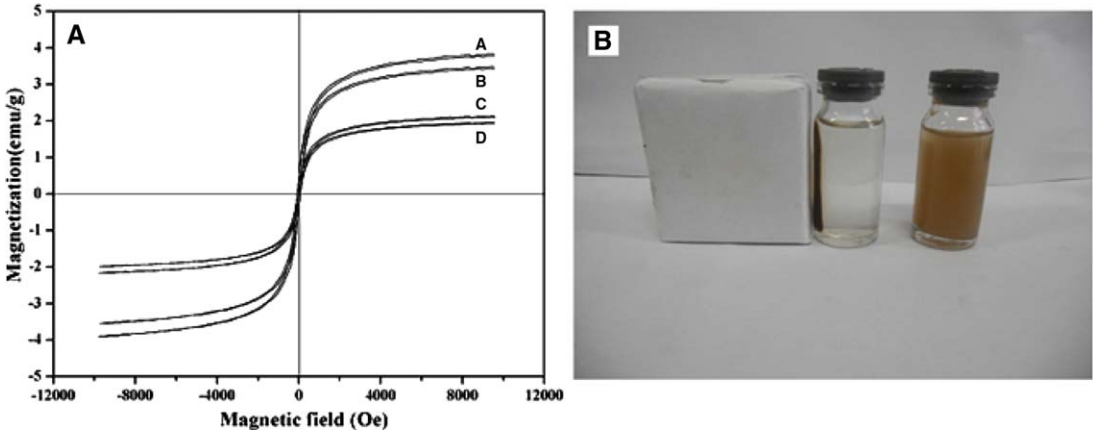

Figure 7. Magnetization curves of MATP (A), V-MATP (B), SMINs (C) and HSMINs (D) at room temperature (A); the photograph of HSMINs suspended in pure water in the absence (right) and in the presence (left) of an external magnet (B). [Color figure can be viewed in the online issue, which is available at wileyonlinelibrary.com.]

with the same initial concentration of 100 μmol L^{-1} at 25°C for 24 h to achieve the adsorption equilibrium, respectively.

The HSMINs (5.0 mg) was placed into SMZ solution (80 μmol L^{-1}) at 25°C for 1.5 h, and were then separated by a magnet. The free SMZ concentration was measured. The saturated HSMINs were extracted by an eluent to remove the SMZ molecules. The cyclic procedures were repeated eight times using the identical batch of HSMINs.

RESULTS AND DISCUSSION

Characterization

FT-IR was used to characterize the ATP, MATP, V-MATP, SMINs, and HSMINs. It can be clearly seen that the peak intensity of O—H stretching of inner hydroxyl groups at 3445 cm^{-1} obviously induced, and the Fe—O peak was very slight at 584 cm^{-1}. The characteristic peak of V-MATP at 1719 cm^{-1} was attributed to C=O stretching vibration, suggesting the successful surface modification of MATP. In the spectra of SMINs

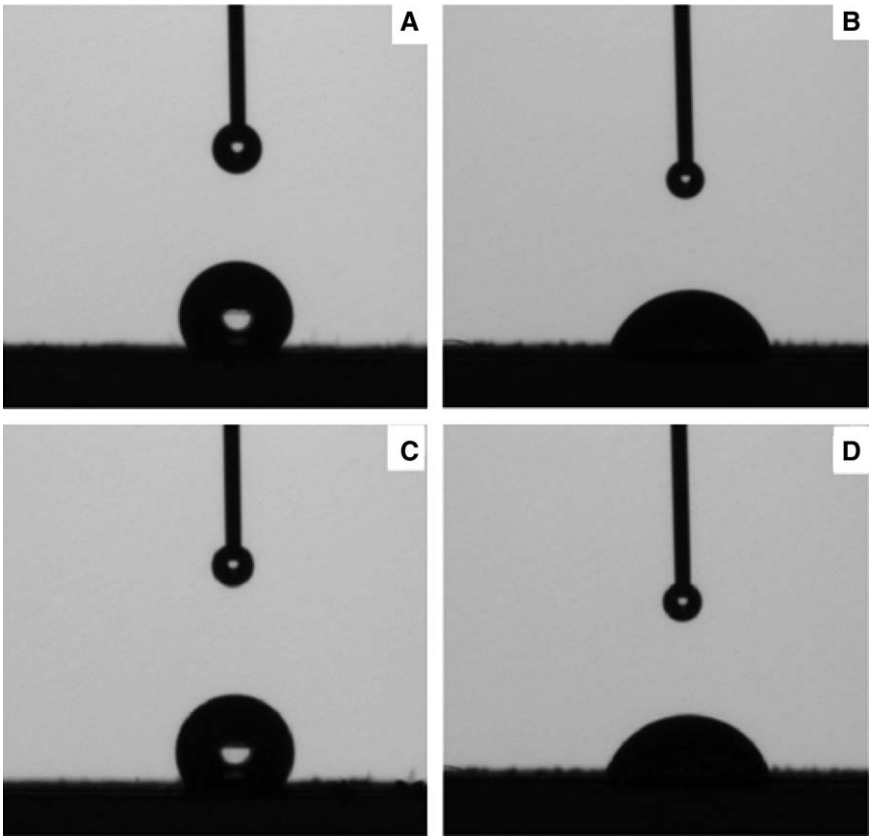

Figure 8. Water contact angle profiles of SMINs (A), HSMINs (B), SNINs (C) and HSNINs (D).

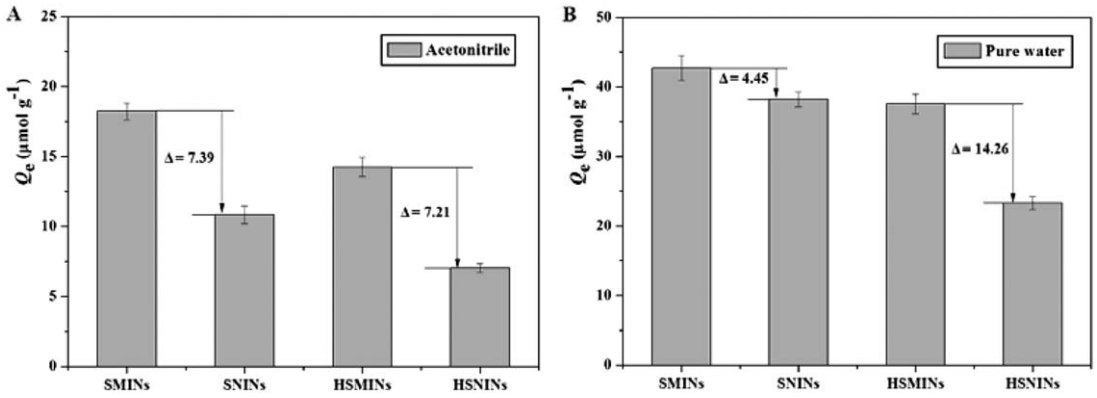

Figure 9. Equilibrium adsorptions of SMZ on SMINs, SNINs, HSMINs and HSNINs in (A) acetonitrile and (B) pure water ($C_o = 50$ μmol L^{-1}) at 25°C, respectively.

in Figure 2(B), the characteristic peaks of C═N stretching in the pyridine rings occurred at 1061 and 1558 cm^{-1}. The absorption bands at 2981 and 2954 cm^{-1} corresponded to the C—H asymmetry stretching vibrations of both —CH_3 and —CH_2 groups, respectively. The absorption peak at 1727 cm^{-1} was corresponded to C═O from EGDMA. The imprinted polymers were successfully coated onto the surface of MATP via RATRPP. As compared with SMINs, some new peaks appeared in the spectra of HSMINs. The broad absorption band at 3445 cm^{-1} was assigned to the stretching vibration of -OH group and the characteristic peaks at 1243 and 1558 cm^{-1} was corresponded to C—O—C stretching, implying PHEMA was grafted onto the SMINs surface as expected.

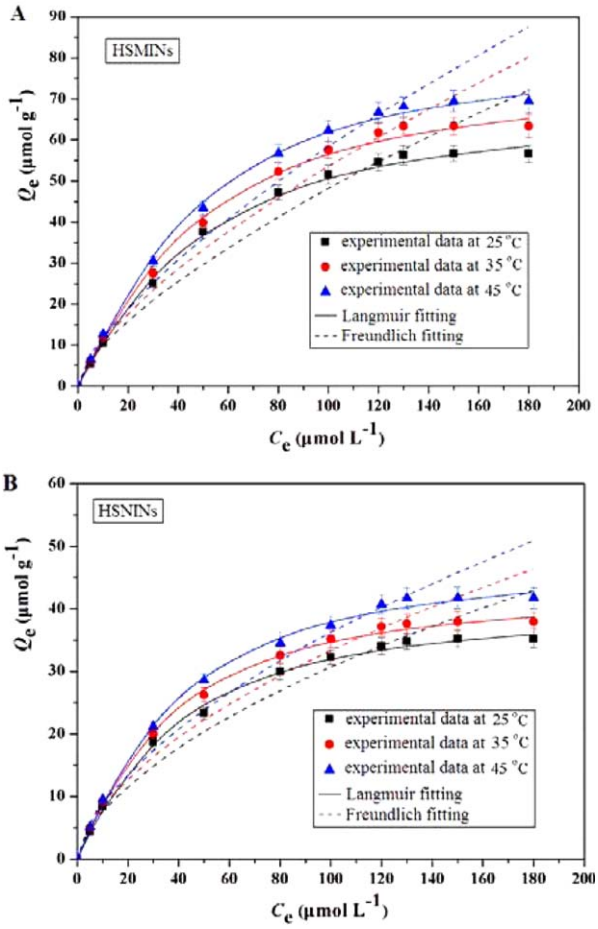

Figure 10. Adsorption isotherm curves of HSMINs (A) and HSNINs (B) toward SMZ. [Color figure can be viewed in the online issue, which is available at wileyonlinelibrary.com.]

SEM was used to observe the morphologies of ATP, MATP, SMINs, and HSMINs. As shown in Figure 3, ATP was rough and fibrous with the length of several hundreds nanometers. Compared with ATP, MATP had a little increase in diameter and stacked together. Figure 3(C) showed that the SMINs presented much lager diameter and smooth surface, due to the successful coating of the polymer layers. The SEM image of HSMINs had no difference with SMINs.

Figure 4 showed the TEM images of ATP, MATP, SMINs, and HSMINs. The morphology of ATP from TEM image was in accordance with the SEM image. As shown in Figure 4(B), magnetic nanoparticles were located on the surface of ATP, the average size of which was about 10 nm. SMINs exhibited the core-shell structure in Figure 4(C), in which the ATP core and polymer nanoshell could be obviously distinguished. The thin imprinting layer was uniform with the thickness of about 14 nm. The average thickness of polymers for HSMINs increased to 15 nm, suggested that HEMA was grafted onto MMINs, thus the hydrophilic polymer brushes was ultrathin.

The crystal structure of ATP and MATP was investigated using XRD and was shown in Figure 5. The presented peaks at 20.7°, 26.6°, and 42.5° were the characteristic peaks of ATP.[43] For MATP, new diffraction peaks of MATP appeared at 30.02°, 36.42°, 44.14°, 57.05°, and 62.76°, which matched with the JCPD standard of magnetite (19–0629 : $2\theta = 30.088°$, 37.071°, 43.07°, 56.958°, and 62.546°). Moreover, the peak intensity of clay slightly decreased. The results demonstrated that magnetic nanoparticles were successfully attached onto ATP.

Figure 6 displayed the TGA curves of MATP, V-MATP, SMINs, and HSMINs, in which the first loss stage in the range from 25 to 250°C was due to the evaporation of physically adsorbed water. For MATP, the second mass loss occurred between

Table I. The Isotherm Constants for Langmuir and Freundlich Isotherm Models

Isotherm models			Langmuir			Freundlich		
Samples	T (°C)	$Q_{e,exp}$ (μmol g^{-1})	Q_m (μmol g^{-1})	K_L (L μmol^{-1})	R^2	K_F [(μmol g^{-1}) (L $\mu mol^{-1})^{1/n}$]	$1/n$	R^2
HSMINs	25	56.65	68.49	0.03853	0.9968	4.313	0.5610	0.9638
	35	63.34	75.76	0.04169	0.9956	5.176	0.5483	0.9708
	45	69.47	81.97	0.04534	0.9976	5.958	0.5399	0.9665
HSNINs	25	35.26	41.32	0.04104	0.9977	3.257	0.5068	0.9620
	35	37.93	43.86	0.04648	0.9980	3.830	0.4908	0.9641
	45	41.73	48.78	0.04341	0.9972	3.977	0.503	0.9716

250 and 500°C was very small (4.43%) from the loss of the inner —OH group, also implying MATP had good thermal stability. The total mass loss of V-MATP (9.94%) was higher than that of MATP (7.37%), suggesting that the MPS was successfully modified. As shown in Figure 6(C,D), the second mass loss of SMINs and HSMINs was 47.8 and 63.4%, respectively, mainly corresponding to the thermal decomposition of imprinted polymer and surface-grafted PHEMA brushes. The consistent weight after 500°C was attributed to the stable MATP, magnetic nanoparticles, and a little residual carbon.

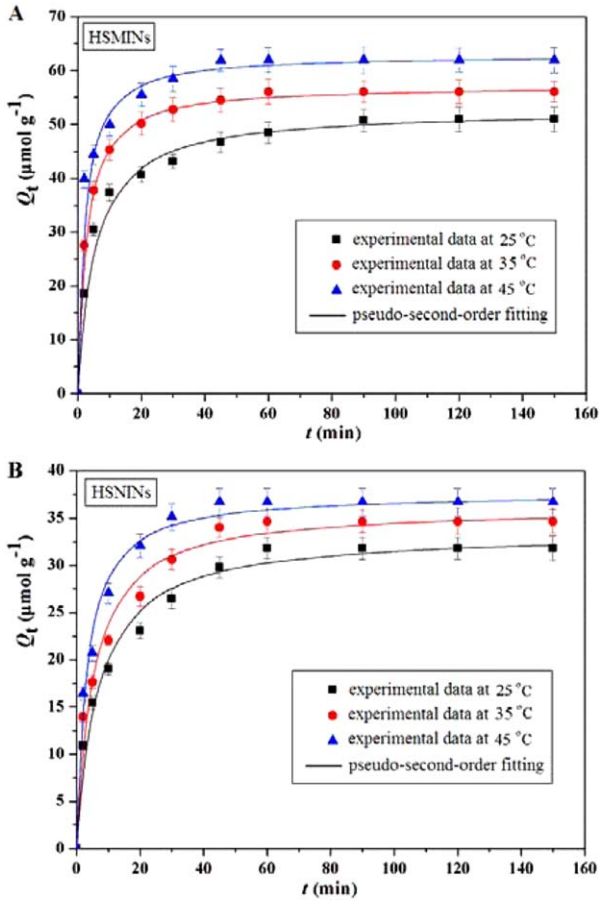

Figure 11. Analysis of kinetics data using the pseudo-second-order kinetic model for HSMINs (A) and HSNINs (B) toward SMZ ($C_o = 80$ μmol L^{-1}). [Color figure can be viewed in the online issue, which is available at wileyonlinelibrary.com.]

In order to further investigate magnetic performance, the magnetic hysteresis loops of MATP, V-MATP, SMINs, and HSMINs were presented in Figure 7(A). It's clear that four curves had similar trend and were symmetrical about the origin without hysteresis, indicating these nanocomposites were superparamagnetic. The saturation magnetization values of MATP and V-MATP was 3.83 and 3.48 emu g^{-1}, respectively, which was in accordance with the result of TGA. The value of SMINs decreased to 2.12 emu g^{-1}, due to the successful coating of imprinted polymer. After the surface-grafting of polymer brushes, the HSMINs had a saturation magnetization value of 1.95 emu g^{-1}, which could meet the magnetic separation. As shown in Figure 7(B), it is clear that HSMINs was uniformly dispersed in pure water (longer than 1.0 h), which benefited from the improvement of surface hydrophilicity. The ungrafted SMINs quickly deposited in the bottle within 5.0 min (not shown). While in the presence of an external magnet, the sample quickly assembled to the wall of the bottle and the solution then turned transparent and clear. All the above results demonstrated that HSMINs could be well used in aquatic solution and be easily separated with the help of an external magnet.

Static water contact angles were tested to further determine the surface-grafting of PHEMA brushes from the SMINs. As shown in Figure 8, the ungrafted SMINs and SNINs were hydrophobic with the static water contact angles 122.2 and 118.9°, respectively. However, the static water contact angles were determined to be 70.6 and 66.2° for HSMINs and HSNINs, respectively. The results obviously showed that the HSMINs exhibited significantly higher surface hydrophilicity than the ungrafted one, again demonstrating the presence of PHEMA brushes on the surface.

Adsorption Properties in Acetonitrile and Pure Water

The equilibrium template adsorption properties of the ungrafted and grafted nanomaterials in acetonitrile were investigated. Both the SMINs and HSMINs could adsorb more SMZ than their corresponding nonimprinted nanomaterials [shown in Figure 9(A)], indicating the presence of selective recognition sites in the prepared SMINs. Note that both the HSMINs and HSNINs exhibited much less adsorption amount toward SMZ than their corresponding ungrafted ones, suggesting again the successful surface-grafting of hydrophilic polymer brushes. Then, the equilibrium adsorption experiments were carried out in the pure water system. As shown in Figure 9(B), the SMINs and SNINs exhibited higher adsorption capacities in water medium than in

Table II. Kinetic Constants for the Pseudo-First-Order and Pseudo-Second-Order Kinetic Model

Kinetic model			Pseudo-first-order			Pseudo-second-order		
Adsorbents	T (°C)	$Q_{e,exp}$ (μmol g^{-1})	$Q_{e,c}$ (μmol g^{-1})	k_1 (min^{-1})	R^2	$Q_{e,c}$ (μmol g^{-1})	k_2 (g μmol^{-1} min^{-1})	R^2
HSMINs	25	51.59	20.39	0.028	0.9342	52.63	0.00396	0.9995
	35	57.58	12.69	0.0191	0.7233	57.14	0.00756	0.9999
	45	62.28	9.608	0.0306	0.7030	62.89	0.00866	0.9998
HSNINs	25	32.26	12.98	0.0289	0.8027	33.44	0.00486	0.9987
	35	35.18	11.27	0.0273	0.7576	36.1011	0.00590	0.9990
	45	37.35	8.063	0.023	0.6487	37.5940	0.00946	0.9996

acetonitrile, mainly due to the high surface hydrophobicity. However, the specific adsorption property of the ungrafted SMINs almost disappeared in pure water. Grafting PHEMA brushes from the surface of SMINs has proven to greatly improve their surface hydrophilicity and enhancing water-compatibility. As expected, the HSMINs showed reduced non-specific adsorption in the pure water system at 25°C [see Figure 9(B)], which thereby demonstrated that the grafting of polymer brushes is an efficient approach for the preparation of water-compatible imprinting to enhance the selective recognition in water system.

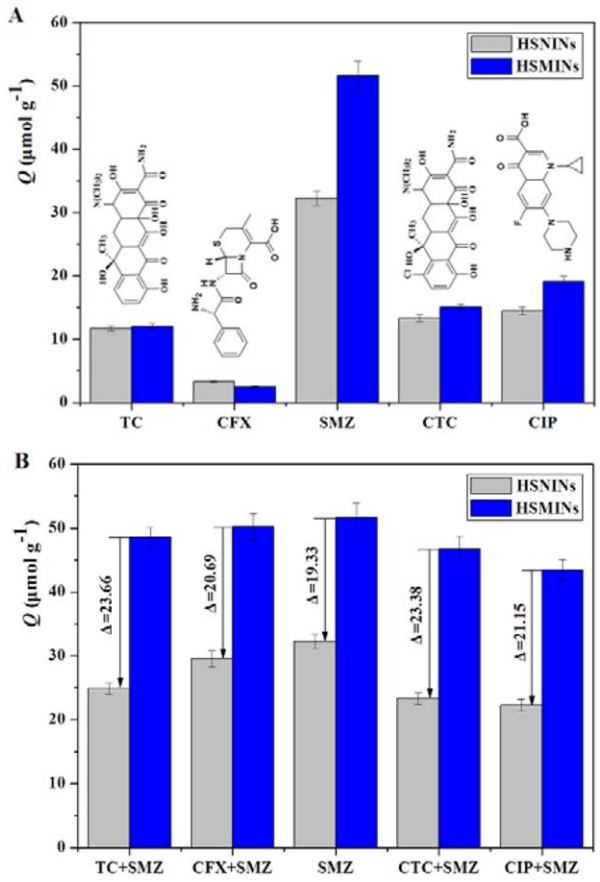

Figure 12. The chemical structure of reference antibiotics and the adsorption amount of HSMINs and HSNINs toward each antibiotic in the single component solution (C_o =100 μmol L^{-1}) (A); the adsorption amount of HSMINs and HSNINs toward SMZ in the binary component solutions (B). [Color figure can be viewed in the online issue, which is available at wileyonlinelibrary.com.]

Adsorption Isotherms

As shown in Figure 10, with the increase of the initial concentration at the same temperature, the adsorption amount of SMZ onto both HSMINs and HSNINs increased and gradually reached the equilibrium. Moreover, the adsorption capacities increased with the increase of the temperature in the whole concentration range, thereby showing the adsorption process to be endothermic in nature. Also, it is clearly that the equilibrium adsorption capacity of HSMINs (56.65, 63.34, and 69.47 μmol g^{-1}) was much higher than that of HSNINs (36.26, 37.93, and 41.73 μmol g^{-1}) at the three temperatures, owing to the specific adsorption for SMZ of imprinting cavies. The adsorption capacity of HSMINs was much larger than the previous SMZ-MIPs by other worker.[44,45]

Here, the Langmuir[46] and Freundlich[47] isotherm models were used to analyze the equilibrium data. The nonlinear form of Langmuir and Freundlich isotherm models are expressed as following equations:

$$Q_e = \frac{K_L Q_m C_e}{1 + K_L C_e} \quad (1)$$

$$Q_e = K_F C_e^{1/n} \quad (2)$$

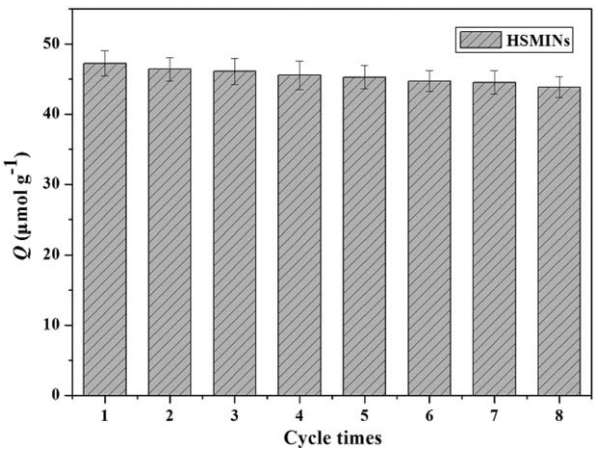

Figure 13. Adsorption capacity of SMZ onto HSMINs under the cyclic procedure.

In eqs. (1) and (2), Q_e (μmol g^{-1}) is the equilibrium adsorption capacity and Q_m (μmol g^{-1}) is the maximum adsorption capacity. K_L (L μmol^{-1}) is the Langmuir adsorption constant. K_F [(μmol g^{-1}) (μmol $L^{-1})^{-1/n}$] and n represent the Freundlich adsorption constants.

Figure 10 showed the fitting curve of adsorption isotherm toward SMZ, and the parameters were listed in Table I. The Freundlich fitting curves for both HSMINs and HSNINs were deviated from the experiment data. Because of the high-correlation coefficient (R^2) value (above 0.995) and the good match between the fitting and experimental value, the experiment data was well-fitted by the Langmuir isotherm model, indicating that adsorption process was monolayer adsorption. The maximum monolayer adsorption capacities of SMZ onto HSMINs in pure water solution were 68.49, 75.76, and 81.97 μmol g^{-1} at 25, 35, and 45°C, respectively, which were 41.32, 43.86, and 48.78 μmol g^{-1} for HSNINs.

Adsorption Kinetics

The adsorption kinetic curves for HSMINs and HSNINs toward SMZ at 25, 35, and 45°C were showed in Figure 10. With the increase of contact time, the adsorption amount quickly increased at first, due to the presence of many empty sites, and subsequently achieved equilibrium. Because the imprinted polymer layer was ultrathin, the adsorption for both HSMINs and HSNINs reached the equilibrium within only 45 min at all three temperatures. Moreover, the higher temperature was in favor for the adsorption equilibrium.

Herein, the pseudo-first-order[48] and pseudo-second-order[49] kinetic models are applied to describe the experimental kinetic data, which are expressed as follows:

$$Q_t = Q_e - Q_e e^{-k_1 t} \tag{3}$$

$$Q_t = \frac{k_2 Q_e^{\,2} t}{1 + k_2 Q_e t} \tag{4}$$

In which k_1 (min^{-1}) and k_2 (g μmol^{-1} min^{-1}) represent the equilibrium rate constants of the pseudo-first-order and pseudo-second-order kinetic models, respectively, which can be calculated from the linear plot of ln Q_e versus ln C_e and t/Q_t versus t, respectively.

Figure 11 displayed the pseudo-second-order kinetic fitting curves of HSMINs and HSNINs, and the fitting parameters were listed in Table II. It is distinctly that R^2 of pseudo-second-order kinetic model for both HSMINs and HSNINs (above 0.999) were much higher than that of pseudo-first-order kinetic model. Besides, the Q_e values calculated from the pseudo-second-order kinetic model were more closed to the experimental ones. From Figure 10, we also can observe that the pseudo-second-order kinetic model fitted the experimental data well. Therefore, the adsorption process for both HMMINs and HMNINs were better fitted by the pseudo-second-order kinetic model, implying the chemical adsorption was the rate-limiting step in the process.[50]

Selectivity Analysis

Here, CIP, TC, CTC, and CFX were chosen as reference antibiotics to investigate the selectivity property of HSMINs for SMZ, the chemical structures of which were displayed in Figure 12(A). The adsorption capacities of each antibiotic onto HSMINs and HSNINs were showed in Figure 12(A). Both HSMINs and HSNINs exhibited higher binding capacities for SMZ than that for other antibiotics. This phenomenon could be possibly explained that the molecule structure of SMZ was smaller with lower steric hindrance and SMZ could form the stronger hydrophobic interaction with the inner polymers. Also, we could see that HSMINs showed high specific adsorption for SMZ (19.33 μmol L^{-1}), due to the imprinted sites matched with template molecules in the structure groups, and however, no specific adsorption for other reference antibiotics. To further investigate the selectivity property, the competitive adsorption experiments in the two-antibiotic solutions were carried out in detail. Figure 12(B) showed the adsorption amount of SMZ onto HSMINs and HSNINs in the presence of other antibiotics. It can be seen that the adsorption capacities of HSMINs toward SMZ had only little decrease, compared with that in the single solutions, exhibiting the good selective recognition ability. The difference values of adsorption amount between the HSMINs and HSNINs for SMZ became larger in the coexistence of competitive antibiotics [in Figure 12(B)]. The experimental results indicated that the successful imprinting of the surfaced specific cavities complemented to SMZ on the surface of MATPs.

Reusability of HSMINs

The reusability of the HSMINs was studied by testing its adsorption capacity to SMZ through the repeated adsorption-desorption procedure, and the stability was a critical element for magnetic separation of the targets from aqueous environments. The result was intuitively showed in Figure 13. The adsorption capacity of HSMINs toward SMZ only decreased by 7.14% after eight cycles, which exhibited the high stability and providing the potentially practical applications in wastewater treatment.

CONCLUSIONS

In conclusion, we successfully prepared a novel surface imprinted core-shell nanoadsorbent with ultrathin PHEMA brushes based on MATP, via a two-step ATRP, with the easy-accessible sites in the imprinted nanoshell. The characterization results indicated the obtained nanoadsorbents exhibited the excellent thermal stability and magnetism, which was convenient to be separated from solution and demonstrated by magnetic separation experiment. The ungrafted SMINs showed no specific adsorption to template in the pure water. The grafting of PHEMA brushes improved the surface hydrophilicity and reduced the nonspecific adsorption in the pure water solutions. The adsorption capacity of the HSMINs toward SMZ increased with the increase of the contact temperatures, and was larger than the previous other's work. The adsorption isotherms were well-described by the Langmuir model, with the maximum monolayer adsorption capacity of 56.65, 63.34, and 69.47 μmol g^{-1} at 25, 35, and 45°C, respectively. Due to the ultrathin polymer shell, the HSMINs exhibited rapid adsorption kinetic property (within 45 min), and the kinetic data was in good accordance with the pseudo-second-order kinetic equation. Also the HSMINs showed the excellent selectivity to SMZ compared with other competitive antibiotics in the single and two-component solutions. The present surface-grafting approach, combine the versatility of ATRP and the availability of various functional monomers, was a general and promising way to prepare water-compatible or multifunctional MIP

for many other templates. Besides, good reusability and stability made this nanoadsorbent be as a potential nanomaterial for practical application in the selective removal of antibiotic residues from water environments.

ACKNOWLEDGMENTS

This work was financially supported by the National Natural Science Foundation of China (Nos. 21176107, 21174057, 21107037, and 21277063), the National Basic Research Program of China (973 Program, 2012CB821500), Natural Science Foundation of Jiangsu Province (BK2011459), Ph.D. Innovation Programs Foundation of Jiangsu Province (No. CXZZ13_0668 and CXLX 12_0646), Research Fund for the Doctoral Program of Higher Education of China (20110205110014), and Jiangsu Planned Projects for Postdoctoral Research Funds (1102119C).

REFERENCES

1. Gehring, T. A.; Griffin, B.; Williams, R. *J. Chromatogr. B* **2006**, *840*, 132.
2. Martinez, J. L. *Science* **2008**, *321*, 365.
3. Chen, L. G.; Zhang, X. P.; Sun, L.; Xu, Y.; Zeng, Q. L.; Wang, H.; Xu, H. Y.; Yu, A. M.; Zhang, H. Q.; Ding, L. *J. Agric. Food Chem.* **2009**, *57*, 10073.
4. Liu, B. H.; Han, M. Y.; Guan, G. J.; Wang, S. H.; Liu, R. Y.; Zhang, Z. P. *J. Phys. Chem. C* **2011**, *115*, 17320.
5. Wuff, G.; Sarhan, A.; Zabrocki, K. *Tetrahedron Lett.* **1973**, *14*, 4329.
6. Vlatakis, G.; Andersson, L. I.; Müller, R.; Mosbach, K. *Nature* **1993**, *361*, 645.
7. Caro, E.; Masqué, N.; Marcé, R. M. *J. Chromatogr. A* **2002**, *963*, 169.
8. Koeber, R.; Fleischer, C.; Lanza, F. *Anal. Chem.* **2001**, *73*, 2437.
9. Martin-Esteban, A. *Fresenius J. Anal. Chem.* **2001**, *370*, 795.
10. Sergeyeva, T. A.; Piletsky, S. A.; J. *Chromatogr. A* **2001**, *907*, 89.
11. Javanbakhta, M.; Attaranb, A. M.; Namjumanesh, M. H. *J. Chromatogr. B* **2010**, *878*, 1700.
12. Byun, H. S.; Youn, Y. N. *Sep. Purif. Technol.* **2010**, *74*, 144.
13. Percival, C. J.; Stanley, S.; Galle, M. *Anal. Chem.* **2001**, *73*, 4225.
14. Hilt, J. Z.; Byrne, M. E. *Adv. Drug Delivery Rev.* **2004**, *56*, 1599.
15. Pasetto, P.; Maddock, S. C.; Resmini, M. *Anal. Chim. Acta* **2005**, *542*, 66.
16. Kempe, H.; Kempe, M. *Anal. Chem.* **2006**, *78*, 3659.
17. Zayats, M.; Lahav, M.; Kharitonov, A. B. *Tetrahedron* **2002**, *58*, 815.
18. Araki, K.; Goto, M.; Furusaki, S. *Anal. Chim. Acta* **2002**, *469*, 173.
19. Guan, G. J.; Liu, R. Y.; Mei, Q. S.; Zhang, Z. P. *Chem. Eur. J.* **2012**, *18*, 4692.
20. Hoon Kim, T.; Do Ki, C.; Cho, H.; Chang, T.; Chang, J. Y. *Macromolecules* **2005**, *38*, 6423.
21. Zhou, W. H.; Lu, C. H.; Guo, X. C.; Chen, F. R.; Yang, H. H.; Wang, X. R. *J. Mater. Chem.* **2010**, *20*, 880.
22. Kan, X. W.; Zhao, Y.; Geng, Z. R.; Wang, Z. L.; Zhu, J. J. *J. Phys. Chem. C* **2008**, *112*, 4849.
23. Pan, J. M.; Yao, H.; Xu, L. C.; Ou, H. X.; Huo, P. W.; Li, X. X.; Yan, Y. S. *J. Phys. Chem. C* **2011**, *115*, 5440.
24. Chen, H.; Wang, A. Q. *J. Colloid Interface Sci.* **2007**, *307*, 309.
25. Zhang, L. X.; Jin, Q. Z.; Shan, L.; Liu, Y. F.; Wang, X. G.; Huang, J. H. *Appl. Clay Sci.* **2010**, *47*, 229.
26. Carter, S. R.; Rimmer, S. *Adv. Funct. Mater.* **2004**, *14*, 553.
27. Xu, S. F.; Li, J. H.; Chen, L. X. *J. Mater. Chem.* **2011**, *21*, 4346.
28. Chang, L. M.; Li, Y.; Chu, J.; Qi, J. Y.; Li, X. *Anal. Chim. Acta* **2010**, *680*, 65.
29. Su, S. F.; Zhang, M.; Li, B. L.; Zhang, H. Y.; Dong, X. C. *Talanta* **2008**, *76*, 1141.
30. Li, Y.; Li, X.; Dong, C. K.; Qi, J. Y.; Han, X. *J. Carbon* **2010**, *48*, 3427.
31. Liu, Y. L.; Huang, Y. Y.; Liu, J. Z.; Wang, W. Z.; Liu, G. Q.; Zhao, R. *J. Chromatogr. A* **2012**, *1246*, 15.
32. Matyjaszewski, K. *Macromolecules* **2012**, *45*, 4015.
33. Wei, X.; Li, X.; Husson, S. M. *Biomacromolecules* **2005**, *6*, 1113.
34. Wei, X.; Husson, S. M. *Ind. Eng. Chem. Res.* **2007**, *46*, 2117.
35. Gai, Q. Q.; Qu, F.; Liu, Z. J.; Dai, R. J.; Zhang, Y. K. *J. Chromatogr. A* **2010**, *1217*, 5035.
36. Yin, J. F.; Cui, Y.; Yang, G. L.; Wang, H. L. *Chem. Commun.* **2010**, *46*, 7688.
37. Dai, J. D.; Pan, J. P.; Xu, L. C.; Li, X. X.; Zhou, Z. P.; Zhang, R. X.; Yan, Y.S. *J. Hazard. Mater.* **2012**, 205, 179.
38. Dirion, B.; Cobb, Z.; Schillinger, E.; Andersson, L. I.; Sellergren, B. *J. Am. Chem. Soc.* **2003**, *125*, 15101.
39. Yang, K.; Berg, M. M.; Zhao, C.; Ye, L. *Macromolecules* **2009**, *42*, 8739.
40. Oxelbark, J.; Legido-Quigley, C.; Aureliano, C. S. A.; Titirici, M. M.; Schillinger, E.; Sellergren, B.; Courtois, J.; Irgum, K.; Dambies, L.; Cormack, P. A. G.; Sherrington, D. C.; De Lorenzi, E. *J. Chromatogr. A* **2007**, *1160*, 215.
41. Pan, G. Q.; Zhang, Y.; Guo, X. Z.; Li, C. X.; Zhang, H. Q. *Biosens. Bioelectron.* **2010**, *26*, 976.
42. Fuertes, A. B.; Tartaj, P. *Chem. Mater.* **2006**, *18*, 1675.
43. Pushpaletha, P.; Lalithambika, M. *Appl. Clay. Sci.* **2011**, *51*, 424.
44. Valtchev, M.; Palm, B. S.; Schiller, M.; Steinfeld, U. *J. Hazard. Mater.* **2009**, *170*, 722.
45. Shi, X. Z.; Meng, Y.; Liu, J. H.; Sun, A. L.; Li, D. X.; Yao, C. X.; Lu, Y.; Chen, J. *J. Chromatogr. B* **2011**, *879*, 1071.
46. Mazzotti, M. *J. Chromatogr. A* **2006**, *1126*, 311.
47. Allen, S. J.; Mckay, G.; Porter, J. F. *J. Colloid Interface Sci.* **2004**, *280*, 322.
48. Ho, Y. S.; McKay, G. *Water Res.* **1999**, *33*, 578.
49. Ho, Y. S.; McKay, G. *Process Biochem.* **1999**, *34*, 451.
50. Baydemir, G.; Andac, M.; Bereli, N.; Say, R.; Denizli, A. *Ind. Eng. Chem. Res.* **2007**, *46*, 2843.